AIP | The Journal of Chemical Physics

Influence of Marangoni flows on the dynamics of isothermal A + B → C reaction fronts

R. Tiani and L. Rongy

Citation: The Journal of Chemical Physics **145**, 124701 (2016); doi: 10.1063/1.4962580
View online: http://dx.doi.org/10.1063/1.4962580
View Table of Contents: http://scitation.aip.org/content/aip/journal/jcp/145/12?ver=pdfcov
Published by the AIP Publishing

Articles you may be interested in

Marangoni-driven convection around exothermic autocatalytic chemical fronts in free-surface solution layers
Chaos **22**, 037106 (2012); 10.1063/1.4747711

Steady Marangoni flow traveling with chemical fronts
J. Chem. Phys. **124**, 164705 (2006); 10.1063/1.2186313

Transient Marangoni convection in hanging evaporating drops
Phys. Fluids **16**, 3738 (2004); 10.1063/1.1772380

On Marangoni convective patterns driven by an exothermic chemical reaction in two-layer systems
Phys. Fluids **16**, 1082 (2004); 10.1063/1.1648641

Three-dimensional numerical simulation of Marangoni flow instabilities in floating zones laterally heated by an equatorial ring
Phys. Fluids **15**, 776 (2003); 10.1063/1.1543147

Reuse of AIP Publishing content is subject to the terms: https://publishing.aip.org/authors/rights-and-permissions. Downloaded to IP: 164.15.136.4 On: Fri, 07 Oct 2016 12:23:06

Influence of Marangoni flows on the dynamics of isothermal A + B → C reaction fronts

R. Tiani[a] and L. Rongy[a]
Nonlinear Physical Chemistry Unit, Faculté des Sciences, Université libre de Bruxelles (ULB), CP231, 1050 Brussels, Belgium

(Received 10 May 2016; accepted 24 August 2016; published online 22 September 2016)

The nonlinear dynamics of A + B → C fronts is analyzed both numerically and theoretically in the presence of Marangoni flows, i.e., convective motions driven by surface tension gradients. We consider horizontal aqueous solutions where the three species A, B, and C can affect the surface tension of the solution, thereby driving Marangoni flows. The resulting dynamics is studied by numerically integrating the incompressible Navier-Stokes equations coupled to reaction-diffusion-convection (RDC) equations for the three chemical species. We show that the dynamics of the front cannot be predicted solely on the basis of the one-dimensional reaction-diffusion profiles as is the case for buoyancy-driven convection around such fronts. We relate this observation to the structure of Marangoni flows which lead to more complex and exotic dynamics. We find in particular the surprising possibility of a reversal of the front propagation direction in time for some sets of Marangoni numbers, quantifying the influence of each chemical species concentration on the solution surface tension. We explain this reversal analytically and propose a new classification of the convective effects on A + B → C reaction fronts as a function of the Marangoni numbers. The influence of the layer thickness on the RDC dynamics is also presented. Those results emphasize the importance of flow symmetry properties when studying convective front dynamics in a given geometry. *Published by AIP Publishing.* [http://dx.doi.org/10.1063/1.4962580]

I. INTRODUCTION

Second-order reactions of the form A + B → C can sustain a front (i.e., a spatially localized region with non-zero production rate) provided that the reactants A and B are initially separated in space. The reaction-diffusion (RD) properties of such fronts have been widely studied in the pioneering work of Gálfi and Rácz[1] and subsequent other theoretical studies.[2–4] Their work was motivated by the knowledge that patterns can be observed in numerous chemical, biological, or physical phenomena in the wake of moving reaction fronts such as the Liesegang structures produced by moving precipitation reaction fronts.[5] Their main results were the exact scaling laws governing the asymptotic one-dimensional (1D) RD dynamics when A and B (with diffusion coefficients D_a and D_b, respectively) react with initial concentrations a_0 and b_0, respectively. In particular, they showed that the position of the front x_f (defined as the position where the production rate is maximum) scales with time as $x_f \sim t^{1/2}$. Danckwerts[6] and Koza[4] further showed that the position of the front in the considered long-time limit is given by $x_f = C_f\sqrt{t}$, where $C_f = C_f(b_0/a_0, D_a, D_b)$ can be calculated numerically. The sign of C_f is determined by the sign of $(a_0\sqrt{D_a})/(b_0\sqrt{D_b}) - 1$, i.e., C_f is positive (negative) when $a_0\sqrt{D_a} > b_0\sqrt{D_b}$ ($a_0\sqrt{D_a} < b_0\sqrt{D_b}$) corresponding to a moving front. $C_f = 0$ when $a_0\sqrt{D_a} = b_0\sqrt{D_b}$ leading to a stationary front.[4] These analytical predictions have been recently extended to the case of initially separated reactants in immiscible solutions.[7]

The scalings described above hold only in the asymptotic diffusion-limited regime when the chemical reaction is limited by the supply of reactants by diffusion, i.e., in the long-time limit (or equivalently for instantaneous reactions $k \to \infty$, where k is the rate constant). Koza and Taitelbaum[8] and Taitelbaum *et al.*[9] have shown that in the non-diffusion-limited or "short-time" regime, the behavior of the system can be characterized by completely different properties. In particular, they demonstrated that under the appropriate choice of initial concentrations and diffusion coefficients, the front exhibits a change in its direction of motion in the course of time. Moreover, they showed that the crossover between the short-time and the long-time limit occurs at a time inversely proportional to the reaction constant. Their analytical findings were supported by numerical integrations of the RD equations.[8] Many experimental works performed in gels to prevent any convective motions are in excellent agreement with the RD theoretical predictions discussed above.[9–12]

However, it has been observed experimentally that, in general, the propagation of chemical fronts in solution can lead to much more complex dynamics than their RD equivalent in gels.[13–31] This observation applies to both the case of A + B → C fronts studied here and the case of autocatalytic fronts. In the latter case, the front separates the products and the reactants of an autocatalytic reaction. Consequently, autocatalytic fronts are self-sustained localized interfaces between miscible solutions with different properties

[a]rtiani@ulb.ac.be and lrongy@ulb.ac.be

Reuse of AIP Publishing content is subject to the terms: https://publishing.aip.org/authors/rights-and-permissions. Downloaded to IP: 164.15.136.4 On: Fri, 07 Oct 2016 12:23:06

(density, surface tension, ...). We note that, on the contrary, the second order A + B → C reaction fronts considered here are not self-organized but result from the particular initial condition of segregated reactants. In both cases, clear discrepancies with classical RD theories were shown to be due to chemically induced convective motions, i.e., hydrodynamic flows induced by gradients of concentration of chemicals. Many studies have been made to understand the resulting pattern instabilities and chemical front dynamics arising from such a chemo-hydrodynamic coupling (see Ref. 28 and references therein). In experiments with horizontal solution layers open to air, fronts are indeed expected to be affected by convective motions driven by surface tension (Marangoni flows) or density (buoyancy flows) gradients across the front arising from concentration and temperature changes during the chemical reaction.[29,30] Buoyancy flows can be easily isolated if the experiment is undertaken in closed systems[30,31] for which no interface with air exists, preventing the possibility to observe Marangoni flows. On the other hand, it is more difficult to isolate Marangoni flows from buoyancy flows unless the experiments are carried out under microgravity conditions. Recent results[32] with autocatalytic fronts of the iodate-arsenous acid reaction have been obtained in parabolic flight experiments in which the gravity field is modulated periodically, allowing to study in particular the relative influence of Marangoni and buoyancy flows on the front dynamics.

In the context of A + B → C fronts, Rongy *et al.*[33] have numerically studied the nonlinear dynamics of those reaction fronts in closed systems, i.e., in the presence of buoyancy-driven flows only. They focused on the case where the reactants A and B have equal diffusion coefficients and equal initial concentrations for which the RD analysis predicts a non-moving front. They found that the symmetry properties of the flow are linked to the symmetry of the depth-averaged density profiles $\langle\rho\rangle(x,t)$ analytically shown to be also functions of the Rayleigh numbers of the problem. They could then classify the observed reaction-diffusion-convection (RDC) dynamics into different regions of the parameter space spanned by the Rayleigh numbers $R_{a,b,c}$ of the species A, B, and C. Further, they extended their results to the case where the reactants have different initial concentrations corresponding to an underlying moving RD front.[34]

Here our objective is to analyze the dynamics of such fronts propagating in systems open to air. We neglect buoyancy effects in order to focus on the coupling between the same second-order kinetic scheme A + B → C, diffusion and Marangoni-driven flows for equal initial concentrations and diffusion coefficients of reactants. Due to the structure of Marangoni flows, the classification of convective effects on RD fronts previously proposed[33] breaks down here. We propose a new classification of the convective dynamics of A + B → C reaction fronts as a function of the Marangoni numbers. In particular, we observe the possibility of a reversal of the front propagation direction in time. Based on analytical arguments, we explain the mechanism leading to such a reversal of the front and predict its occurrence as a function of the Marangoni numbers. The influence of the layer thickness on the RDC dynamics is also discussed.

The article is organized as follows. In Section II, we present the model system and the corresponding governing dimensionless equations. The nonlinear dynamics of the system is described in Section III. Eventually, conclusions and prospects are drawn in Section IV.

II. MODEL SYSTEM

We consider a two-dimensional (2D) thin aqueous solution layer of length L_x and height L_z oriented horizontally in the gravity field $\underline{g}$ and open to air. The isothermal A + B → C reaction takes place upon contact between two miscible aqueous solutions, each containing one of the reactants (see Fig. 1). The reactants A and B are brought into contact along a planar vertical interface located at $x = 0$ at initial concentrations a_0 and b_0, respectively. The reactants and the product affect the surface tension of the solution, thereby inducing gradients of surface tension leading to Marangoni flows. We assume no surface deformation and no evaporation, so that we do not address the dynamics in the air layer. In order to focus on Marangoni effects, we furthermore neglect any buoyancy-driven flow, considering the solution density as constant in space and time. The governing equations for this system are therefore obtained by coupling the RDC equations for the concentrations of the reactants a, b and of the product c coupled to the 2D incompressible Navier-Stokes equations for the velocity field $\underline{v} = (u, w)$. The model reads

$$\frac{\partial a}{\partial t} + \underline{v}.\underline{\nabla}a = D\nabla^2 a - kab, \tag{1}$$

$$\frac{\partial b}{\partial t} + \underline{v}.\underline{\nabla}b = D\nabla^2 b - kab, \tag{2}$$

$$\frac{\partial c}{\partial t} + \underline{v}.\underline{\nabla}c = D\nabla^2 c + kab, \tag{3}$$

$$\frac{\partial \underline{v}}{\partial t} + (\underline{v}.\underline{\nabla})\underline{v} = \nu\nabla^2\underline{v} - \frac{1}{\rho_0}\underline{\nabla}p + \underline{g}, \tag{4}$$

$$\mathrm{div}\,\underline{v} = 0, \tag{5}$$

where p denotes the pressure and $\underline{g} = (0, -g)$ is the gravity acceleration. All chemical species are assumed to have the same constant diffusion coefficient D. The solution density ρ_0, the fluid kinematic viscosity $\nu = \mu/\rho_0$, where μ is the dynamic viscosity, and the rate constant k are assumed constant.

Our rectangular system has rigid side walls, a rigid bottom, and a free upper surface. At each boundary of the domain, we require zero-flux boundary conditions for the chemical concentrations. The boundary conditions for the fluid velocity field at the rigid boundaries are no-slip conditions,

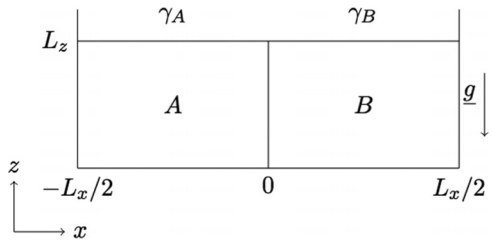

FIG. 1. Sketch of the system.

Reuse of AIP Publishing content is subject to the terms: https://publishing.aip.org/authors/rights-and-permissions. Downloaded to IP: 164.15.136.4 On: Fri, 07 Oct 2016 12:23:06

$u = 0$ and $w = 0$. At the free surface, we require $w = 0$ and we use a Marangoni boundary condition for the horizontal fluid velocity u,

$$\mu \frac{\partial u}{\partial z} = \frac{\partial \gamma}{\partial x} \text{ at } z = L_z, \tag{6}$$

where γ is the surface tension of the solution. This expresses the fact that Marangoni effects drive a non-zero horizontal fluid velocity u when a horizontal surface tension gradient exists.[35]

To non-dimensionalize the problem, we use the characteristic scales of the reaction-diffusion system: for time, $\tau_c = 1/ka_0$, length $L_c = \sqrt{D\tau_c}$, velocity $U_c = L_c/\tau_c = \sqrt{D/\tau_c}$, and concentration a_0. The pressure is scaled by $p_c = \mu/\tau_c = \rho_0 S_c D$, where the dimensionless parameter $S_c = \nu/D$ is the Schmidt number and we defined a new dimensionless pressure gradient incorporating the hydrostatic pressure gradient as $\underline{\nabla}' p' = \underline{\nabla}' p/p_c - \rho_0 L_c \underline{g}/p_c$ where the primes denote dimensionless variables. The dimensionless surface tension is defined as $\gamma' = (\gamma - \gamma_0)/\gamma_c$, where $\gamma_c = p_c L_c$, and γ_0 is the surface tension of the solvent. Dropping all the primes, we obtain the following dimensionless governing equations:

$$\frac{\partial a}{\partial t} + \underline{v}.\underline{\nabla} a = \nabla^2 a - ab, \tag{7}$$

$$\frac{\partial b}{\partial t} + \underline{v}.\underline{\nabla} b = \nabla^2 b - ab, \tag{8}$$

$$\frac{\partial c}{\partial t} + \underline{v}.\underline{\nabla} c = \nabla^2 c + ab, \tag{9}$$

$$\frac{\partial \underline{v}}{\partial t} + (\underline{v}.\underline{\nabla})\underline{v} = S_c(\nabla^2 \underline{v} - \underline{\nabla} p), \tag{10}$$

$$\text{div}\, \underline{v} = 0, \tag{11}$$

with boundary conditions,

$$\frac{\partial c_i}{\partial x} = u = w = 0 \text{ at } x = \pm L_x/2, \tag{12}$$

$$\frac{\partial c_i}{\partial z} = u = w = 0 \text{ at } z = 0, \tag{13}$$

$$\frac{\partial c_i}{\partial z} = w = 0 \text{ at } z = L_z, \tag{14}$$

$$\frac{\partial u}{\partial z} = -\sum_i M_i \frac{\partial c_i}{\partial x} \text{ at } z = L_z, \tag{15}$$

where L_x and L_z now represent, respectively, the dimensionless length and height of the layer. The condition (15) is the dimensionless form of Eq. (6) and introduces the dimensionless solutal Marangoni number of the corresponding species i $(i = a, b, c)$ quantifying the influence of each chemical species concentration on the solution surface tension,

$$M_i = -\frac{1}{\mu}\sqrt{\frac{a_0}{Dk}}\frac{\partial \gamma}{\partial c_i}. \tag{16}$$

Note that the solutal Marangoni numbers M_a, M_b, M_c will be positive throughout our study because the corresponding solutes here are all supposed to decrease the surface tension of the solvent.

We suppose a linear dependence between the surface tension and c_i, $\gamma = \gamma_0 + \sum_i (\partial\gamma/\partial c_i)c_i$. The Marangoni numbers, M_i, are therefore constant and specific to each species i. The dimensionless surface tension of the solution is given by

$$\gamma(x,t) = -M_a a(x, L_z, t) - M_b b(x, L_z, t) - M_c c(x, L_z, t). \tag{17}$$

The initial conditions are separated reactants such that

$$a = 1,\ b = 0,\ c = 0,\ \forall z,\ x \le 0, \tag{18}$$

$$a = 0,\ b = 1,\ c = 0,\ \forall z,\ x > 0, \tag{19}$$

i.e., the initial concentrations of species A and B are chosen as equal ($a_0 = b_0$).

We numerically integrate Eqs. (7)-(11) subjected to the boundary and initial conditions described above using the numerical procedure explained in the work of Rongy *et al.*[36] The solutions of those equations were found to converge on decreasing the temporal and spatial step sizes. Typically the spatial step sizes are $dx = 0.5$ and $dz = 0.25$. The corresponding time step is $dt = 8 \times 10^{-6}$. Our model includes six dimensionless parameters: four hydrodynamic parameters, the Marangoni numbers of each species $M_{a,b,c}$ and the Schmidt number S_c, and two parameters related to the domain geometry, L_x and L_z. The length L_x is chosen sufficiently large so that the results are not affected by boundary effects on the time of interest, typically $L_x = 300$. The typical Schmidt number for small species in water at room temperature is equal to $S_c = \mu/\rho_0 D \approx 10^3$. It has been shown to have no influence on Marangoni driven flows around chemical fronts, provided it is taken in the experimental range $S_c \in [4.5 \times 10^2, 1.3 \times 10^3]$ meaning that we effectively analyze a Stokes flow.[36] In this paper, we investigate the influence of the domain height L_z and the Marangoni numbers on the front dynamics. It is important to note that the dynamical properties of the front presented here are not restricted to the chosen Marangoni numbers. We have verified indeed that such properties do not change for all the tested Marangoni numbers $(M_a, M_b, M_c) \le 300$ and domain heights $L_z \le 25$.

III. CLASSIFICATION OF MARANGONI-DRIVEN NONLINEAR DYNAMICS

The numerical study of the RDC dynamics for various sets of Marangoni numbers shows that the number of convective rolls, their relative size, and rotational direction can all be predicted on the basis of the surface tension profiles, which present the same monotonic properties as the RD surface tension profiles for all times. This is similar to the density profiles in the case of buoyancy-driven convection.[33] Indeed, as the flow field is driven by the horizontal surface tension gradient, two convective rolls are observed when γ is nonmonotonic, i.e., its gradient γ_x changes sign in the x direction. On the contrary, a single convective roll is present when γ is monotonic, i.e., its gradient γ_x is single-signed. This monotonic feature of γ can be predicted as a function of the Marangoni numbers without resorting to numerics by a simple 1D RD analysis. Indeed the sum (7) + (8) + 2 × (9) with $\underline{v} = \underline{0}$ shows that $a + b + 2c$ obeys a diffusion

Reuse of AIP Publishing content is subject to the terms: https://publishing.aip.org/authors/rights-and-permissions. Downloaded to IP: 164.15.136.4 On: Fri, 07 Oct 2016 12:23:06

equation,

$$\frac{\partial(a+b+2c)}{\partial t} = \nabla^2(a+b+2c). \tag{20}$$

With the initial conditions (18) and (19) and the boundary conditions (12)-(15), this variable equals 1 everywhere at $t = 0$ and therefore $a + b + 2c$ equals 1 for all times. Thus $c(x,t) = \frac{1}{2}[1 - a(x,t) - b(x,t)]$, allowing to reconstruct the surface tension as

$$\gamma(x,t) = -\frac{M_c}{2} - \left(M_a - \frac{M_c}{2}\right) a(x,t) - \left(M_b - \frac{M_c}{2}\right) b(x,t). \tag{21}$$

Taking its derivative with regard to x, we obtain

$$\gamma_x(x,t) = -\left(M_a - \frac{M_c}{2}\right) a_x(x,t) - \left(M_b - \frac{M_c}{2}\right) b_x(x,t). \tag{22}$$

Since the gradients of a and b are single-signed, $a_x \leq 0$ and $b_x \geq 0$, γ_x is also single-signed when M_c lies between $2M_a$ and $2M_b$. Whenever M_c lies outside that range, the two terms of Eq. (22) have opposite sign. Therefore we conclude that the surface tension profile is nonmonotonic whenever M_c is outside the range between $2M_a$ and $2M_b$. In Fig. 2 a sketch of the six different types of surface tension profiles is shown in the (M_b, M_c) plane at fixed M_a. We note that the surface tension profiles corresponding to the solid line $M_a = M_b$ have not been sketched for clarity. The shaded regions corresponding to $2M_a < M_c < 2M_b$ or $2M_b < M_c < 2M_a$ indicate when surface tension profiles are monotonic, leading to a single convective roll. This single convective roll is initiated at the surface towards the zone with the largest surface tension. When $M_b < M_a$, $\gamma_b > \gamma_a$ and the convective roll turns clockwise. When $M_b > M_a$, $\gamma_b < \gamma_a$ and the convective roll turns counterclockwise. The unshaded regions feature nonmonotonic surface tension profiles for which two counter-rotating convective rolls are observed. In particular, if $M_c = 2M_a = 2M_b$, Eq. (21) shows that the surface tension is constant everywhere, no fluid flow is obtained ($\underline{v} = 0$), and the planar RD stationary front is recovered. Such a case corresponds to the intersection point between the solid and broken lines in Fig. 2.

As already mentioned above, we have numerically verified that the RDC surface tension profiles present the same monotonic properties than the ones drawn in Fig. 2 from the RD concentration profiles for all times. This is illustrated in Fig. 3 for some sets of Marangoni numbers. The corresponding flow field superimposed on the production rate, ab, is illustrated in Fig. 4 for some of these sets representative of regions I, II, and III of Fig. 3 as well as for the solid line ($M_a = M_b$) for $M_c < 2M_a$. The structure of the flow field confirms the predictions of the above analysis (Fig. 2). We note that the Marangoni flows have deformed the planar geometry of the RD front independently of the observed number of convective rolls. We also notice that the maximum of the production rate tends to be localized at the convergence points between the two convective rolls in Figs. 4(a)-4(c) while it is around the middle when one convective roll is observed as in Fig. 4(d).

We recall that the position of the front is defined as the position where the production rate ab is maximum. Although two coordinates x and z are necessary to define this point properly in our 2D geometry, the x coordinate is more important when dealing with moving fronts. We therefore define the front position X_f, as the point where the depth-averaged production rate $\langle ab \rangle$ reaches its maximum. The depth-averaged quantities are all defined as

$$\langle \phi \rangle(x,t) = \frac{1}{L_z} \int_0^{L_z} \phi(x,z,t) dz, \tag{23}$$

where ϕ stands for the considered field (a, b, c or ab). We note that the numerical uncertainty on the measure of the position of the front is $dx/2$ with $dx = 0.5$.

We can now consider the influence of Marangoni-driven convection on the front dynamics for equal initial concentrations and diffusion coefficients of reactants corresponding to a stationary planar RD front. Since the approach used

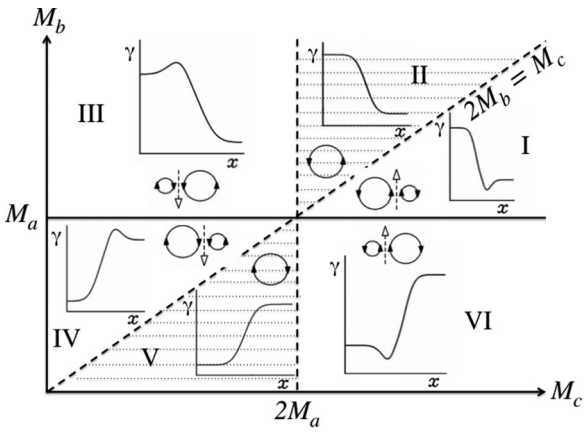

FIG. 2. Typical surface tension profiles along with a sketch of the expected convective rolls are illustrated within the corresponding regions in the parameter (M_b, M_c) plane at fixed M_a. The shaded region corresponds to monotonic surface tension profiles with one single vortex. Outside the shaded region, nonmonotonic surface tension profiles induce two vortices. The arrow on the circles indicate the rotation direction of the vortices.

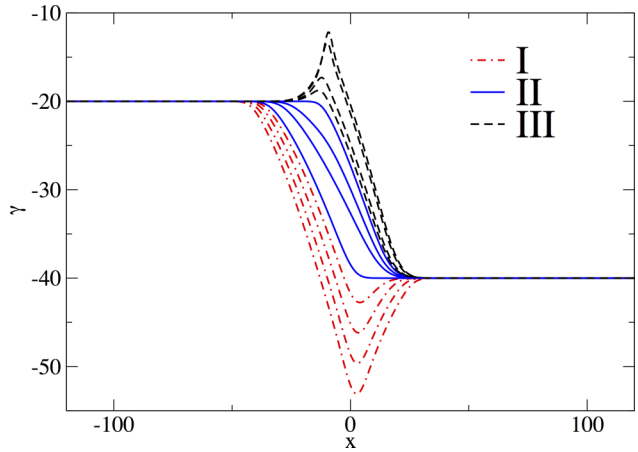

FIG. 3. Numerical surface tension profiles along x at $t = 30$ for $M_a = 20$, $M_b = 40$, and $M_c = 10$, 15, 30, 35, 40, 50, 60, 80, 90, 100, 110, 120 from top to bottom. Those profiles are reconstructed from Eq. (17) where the concentrations a, b, c are solutions of Eqs. (7)-(15).

Reuse of AIP Publishing content is subject to the terms: https://publishing.aip.org/authors/rights-and-permissions. Downloaded to IP: 164.15.136.4 On: Fri, 07 Oct 2016 12:23:06

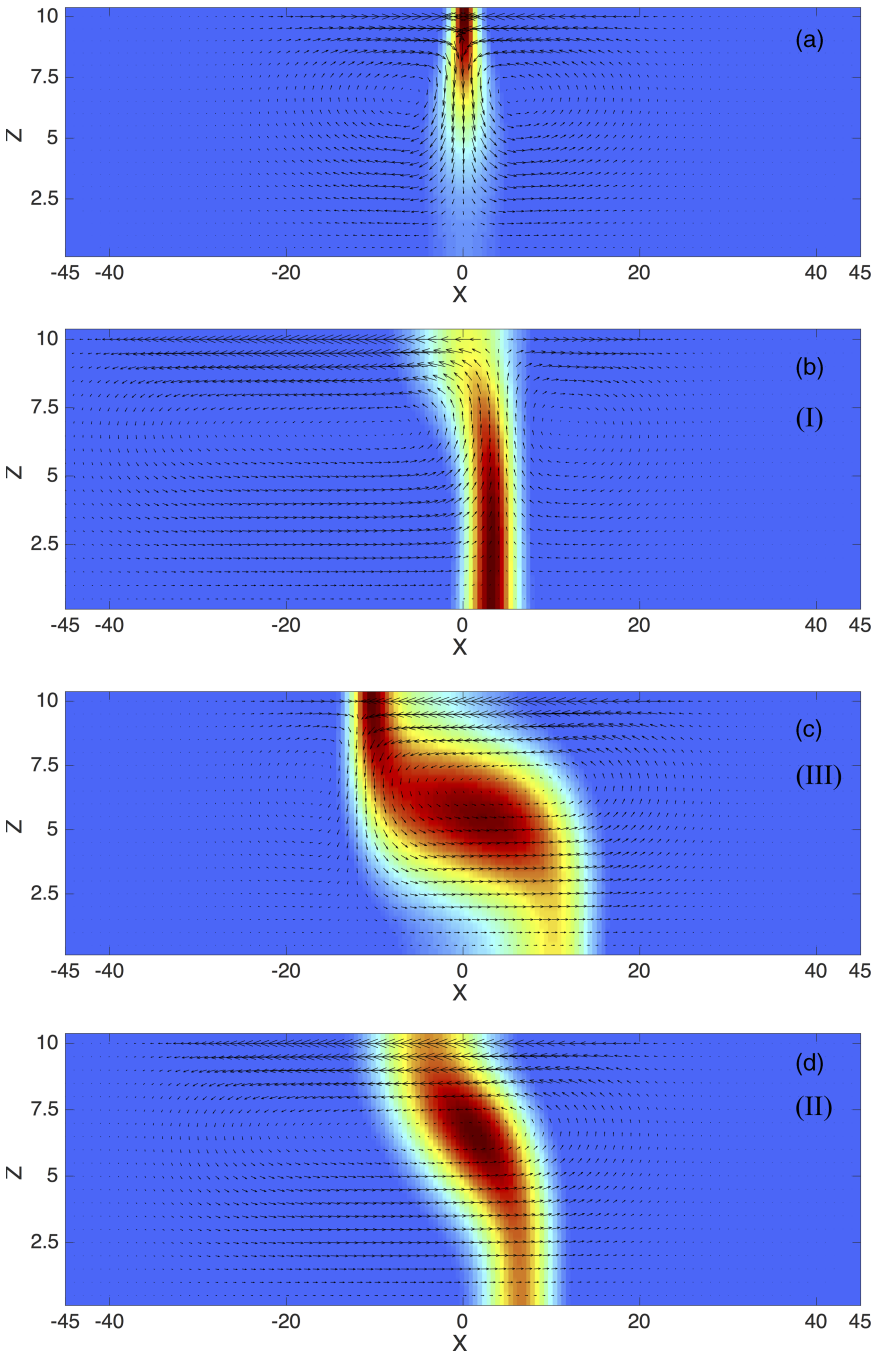

FIG. 4. Focus on the convective rolls centered on the deformed reaction front shown at $t = 30$. The fluid velocity field is superimposed on a 2D plot of the production rate which ranges between its maximum value, ab_{max} shown in red, and its minimum value, $ab_{min} = 0$, shown in blue. The z-direction has been magnified to see the details of the velocity field. The velocity vectors are here tripled compared to their effective length to allow for a better visualization. The figures shown here correspond from top to bottom to (a) $M_a = M_b = 40, M_c = 30$, and $ab_{max} = 0.050$, (b) $M_a = 20, M_b = 40$, $M_c = 100$, and $ab_{max} = 0.035$, (c) $M_a = 20, M_b = 40, M_c = 25$, and $ab_{max} = 0.014$, and (d) $M_a = 20, M_b = 40$, $M_c = 60$, and $ab_{max} = 0.018$. The last three figures are associated to the regions I, III, and II of Fig. 3, respectively.

to interpret the evolution of the reaction front is different in the presence of one or two convective rolls, we propose to analyze in Subsections III A and III B the nonlinear dynamics of the front for these two cases separately. We also study the influence of the dimensionless height L_z in both cases. Moreover, since the symmetry properties of the surface tension profiles of upper regions (I, II, III) are unchanged when performing the transformation $M_a \leftrightarrow M_b$ in Fig. 2, the front dynamics of the lower regions (IV, V, VI) can easily be deduced from the upper regions. Therefore, the results for the front dynamics are arbitrarily shown for the upper regions in Subsections III A and III B without loss of generality. The general classification of the front dynamics is then drawn in Subsection III C as a function of all the Marangoni numbers.

A. Front dynamics in the presence of two convective rolls (regions I and III)

The simplest case to consider is when $M_a = M_b$ for any value of M_c for which the surface tension profiles are symmetric along x leading to two identical convective rolls (see Fig. 4(a)). In that case, denoted by the solid line in Fig. 2, the intensity of the flow is equal on the left and right sides and the reaction front remains immobile ($X_f = 0, \forall t$). Note that without the chemical reaction, the surface tension would be constant everywhere for all times and no fluid flow would therefore be observed. For all the other Marangoni numbers taken in the unshaded regions of Fig. 2 where two convective rolls are observed, the surface tension profiles are asymmetric

Reuse of AIP Publishing content is subject to the terms: https://publishing.aip.org/authors/rights-and-permissions. Downloaded to IP: 164.15.136.4 On: Fri, 07 Oct 2016 12:23:06

along x leading to an asymmetric flow fluid, and the front moves.

1. Region I: The surface tension profiles have a minimum

Fig. 5(a) shows the position of the front for fixed M_a, M_b and different M_c lying within region I where the surface tension profiles present a minimum in the reaction zone. In that case, the product C reduces the surface tension of the solvent more than the reactants. Since the surface tension gradient is stronger on the left side, convection is more intense on this side pushing the reaction front in the opposite direction leading to positive values for the position of the front $X_f > 0$. By considering the flow field in Fig. 4(b), we observe that the reaction front has moved towards the right ($X_f > 0$), i.e., from the side where the strongest convective roll is observed to the side of the weakest one. When M_c increases, both convective rolls grow in intensity but the relative difference in their size decreases. Therefore the front propagates less further when M_c increases as shown in Fig. 5(a). We expect that $X_f \to 0$ when $M_c \to \infty$, $\forall(M_a, M_b)$. The influence of the layer thickness on the motion of the front is illustrated in Fig. 5(b). The larger L_z, the stronger the convection and the larger the magnitude of the position of the front due to the decrease of the influence of the no-slip boundary condition at the bottom.

2. Region III: The surface tension profiles have a maximum

Next, we study the case where the surface tension profiles present a maximum in the reaction zone because C reduces the surface tension of the solvent less than reactants A and B (region III). As for the previous case, the production rate is maximum where the two convective rolls converge (here at the surface, see Fig. 4(c)). Nevertheless, the reaction front is deformed across the whole thickness. This can be explained by considering the space-time evolution of the 2D front (production rate) and the concentration field of one of the reactants A shown in Fig. 6. While the net force at the surface is oriented to the left, the different plots show that the return flow (of the strongest convective roll) initially displaces a

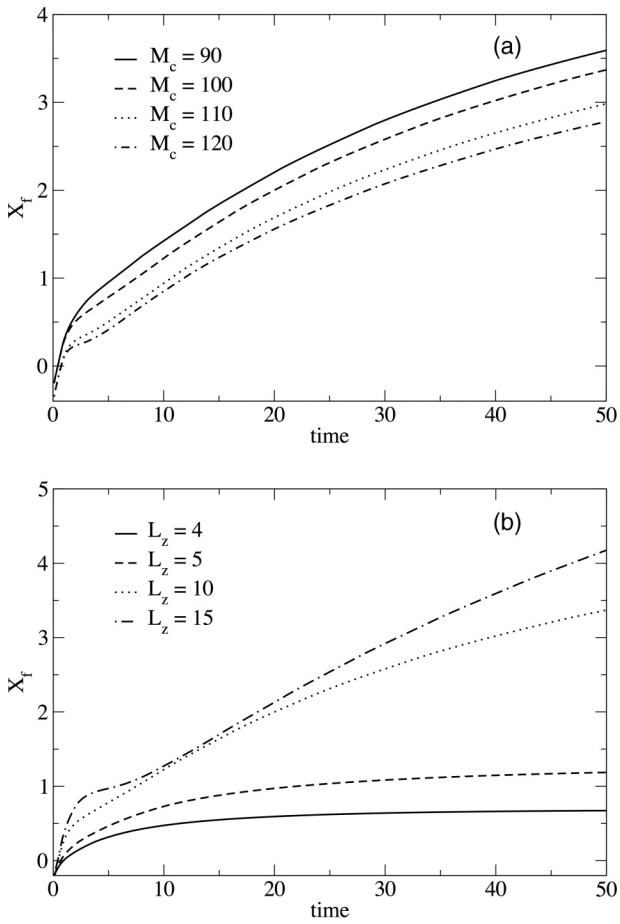

FIG. 5. Position of the reaction front X_f against time corresponding to the case where the surface tension profiles present a minimum in the reaction zone (region I) illustrated for (a) $M_a = 20$, $M_b = 40$, and various values of M_c for a fixed layer thickness ($L_z = 10$) and (b) for $M_a = 20$, $M_b = 40$, $M_c = 100$, and different values of L_z.

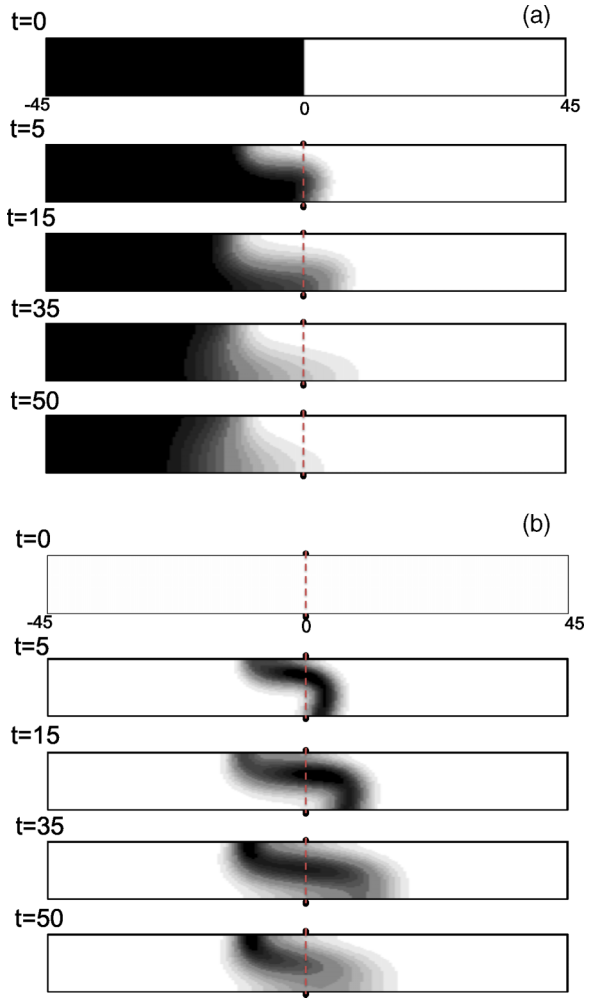

FIG. 6. Space-time evolution of the concentration field of (a) the reactant A and (b) production rate ab for $M_a = 20, M_b = 40$, and $M_c = 25$ (region III). The layer is shown between $x = -45$ and $x = 45$ and the aspect ratio with the layer thickness ($L_z = 10$) is preserved. Dark regions correspond to high concentrations (or production rate) with the maximum in black and the minimum in white.

Reuse of AIP Publishing content is subject to the terms: https://publishing.aip.org/authors/rights-and-permissions. Downloaded to IP: 164.15.136.4 On: Fri, 07 Oct 2016 12:23:06

considerable amount of A in the opposite direction where it reacts with B, increasing the production rate in the bulk and deforming therefore the reaction front across the depth. Due to the deformation of the reaction front, the usual definition of the front position (as the position of the maximum of the depth-averaged production rate) does not reflect the front dynamics at the surface. Therefore, we introduce X_f^* as the new position of the front defined as the position of the maximum production rate at the surface (see Fig. 7). Fig. 7(a) confirms that the front moves initially towards the side with the less intense flow. As time increases, convection gets weaker as the surface tension gradients decrease in time. Hence, the reaction front slows down and eventually changes direction to return to its initial position because diffusion takes over (large-time diffusive limit predicted by Gálfi and Rácz[1]). Increasing L_z makes the front move faster without affecting its qualitative evolution (see Fig. 7(b)). If we compare the evolution of the front in Fig. 5, we observe that the motion of the front is smaller and less sensitive to the increase of the height domain L_z in region I. This is due to the fact that the front is localized at the convergence point of the two convective rolls. The latter is in the bulk closer to the bottom of the system and then more strongly influenced by the no-slip condition $\underline{v} = 0$ slowing down its motion. Moreover, for the same reason, the time scale of the front dynamics is longer and the diffusive limit is then reached much later in region I than in region III. Finally, note that the amount of reactant B pushed (by the strongest convective roll) in the opposite direction to the front propagation in region I is too small to observe a similar deformation than in region III explaining the difference in the observed front dynamics between those two regions.

B. Front dynamics in the presence of a single convective roll (region II)

We now turn to region II where the surface tension profiles are monotonic, leading to a single convective roll. As observed in Fig. 4(d), since there is only one convective roll, the front is not particularly localized at a given position so that we have to use the usual definition for the position of the front given by the maximum of $\langle ab \rangle$. For all sets of Marangoni numbers (M_a, M_b, M_c) in that region, the surface tension profiles are seen asymmetric and therefore, the front moves (see Fig. 8). Surprisingly the front reverses its direction in time for some sets of Marangoni numbers (see Fig. 8(a)). We also notice that the time at which the front reversal occurs increases with M_c. Similarly to the case where two convective rolls are observed,

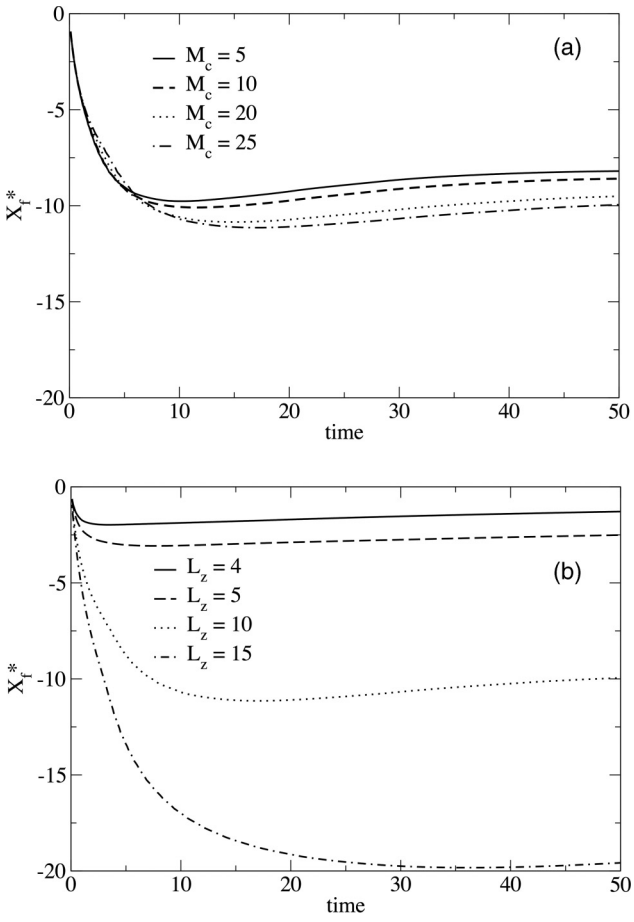

FIG. 7. Position of the reaction front at the surface X_f^* against time corresponding to the case where the surface tension profiles present a maximum in the reaction zone (region III) illustrated for (a) $M_a = 20$, $M_b = 40$, and various values of M_c for a fixed layer thickness ($L_z = 10$) and (b) $M_a = 20$, $M_b = 40$, $M_c = 10$, and different values of L_z.

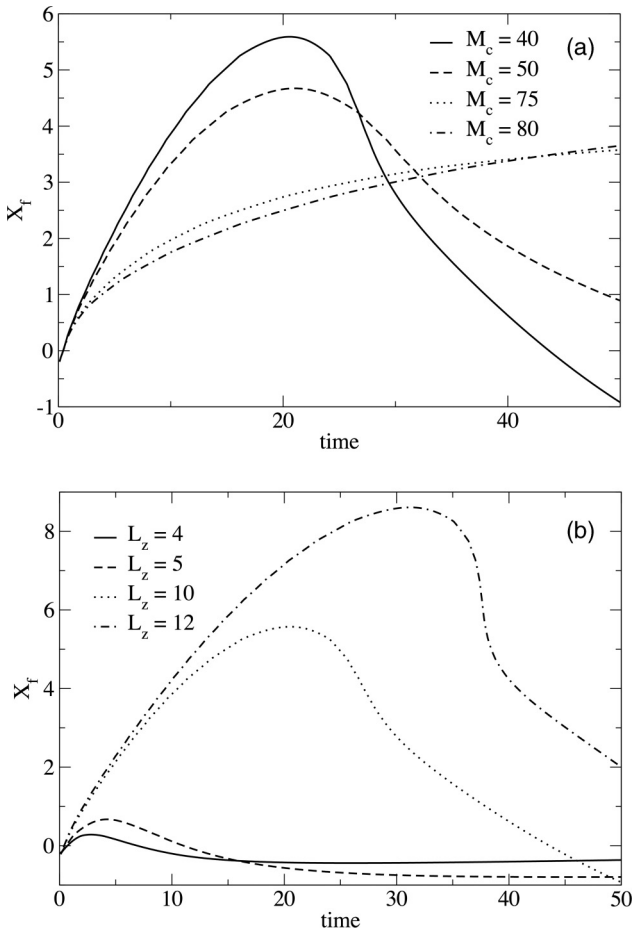

FIG. 8. Position of the reaction front X_f against time when the surface tension profile is monotonic (region II) for (a) $M_a = 20$, $M_b = 40$, and various values of M_c for a fixed layer thickness ($L_z = 10$) and (b) different values of L_z for $M_a = 20$, $M_b = 40$, and $M_c = 40$.

Reuse of AIP Publishing content is subject to the terms: https://publishing.aip.org/authors/rights-and-permissions. Downloaded to IP: 164.15.136.4 On: Fri, 07 Oct 2016 12:23:06

Fig. 8(b) shows, moreover, that the layer thickness affects the dynamics of the system quantitatively but not qualitatively. Such a reversal cannot be explained solely on the basis of the surface tension profiles. We then propose an analytical explanation based both on the surface tension profiles and the structure in depth of the convective roll that we describe below.

Since in the present case $\gamma_A > \gamma_B$, the Marangoni flow structure can be seen as a flow initiated at the surface and oriented towards A plus a return flow acting in the opposite direction arising from the incompressibility condition. It is numerically observed that the flow changes its direction around $z = 2L_z/3$ for all the values of L_z we have screened, corresponding to the approximation of a parallel flow $\underline{v} = (u(z),0)$, schematized in Fig. 9.[35] Reactant B is pushed to the left due to the action of the flow near the surface ($2L_z/3 < z < L_z$) while reactant A is brought to the right due to the action of the return flow in the lower part ($0 < z < 2L_z/3$).

For all the Marangoni numbers tested in region II, it is interesting to note that the front always moves initially to the right. Indeed in the short-time limit, the asymmetry of the surface tension profiles is weak so that the front initially propagates to the right simply because of the large amount of A molecules displaced compared to B molecules (see Fig. 9). As time increases, the concentration of C increases, thereby increasing the asymmetry of the surface tension profiles along x and of the resulting flow. If the intensity of the flow on the right ($x > X_f$) is large enough compared to the one on the left ($x < X_f$), a reversal of the front propagation direction might be observed. An evolution equation for the relative intensity of the flow around the front is then needed to predict for which Marangoni numbers such a front reversal occurs. Although the exact relation between the relative intensity of the flow around the front and the Marangoni numbers is not known, it can be observed that in the presence of two convective rolls, for instance in region I, the front basically moves to the right in the direction of the less intense flow when the surface tension difference $|\gamma_A - \gamma(X_f,t)| > |\gamma(X_f,t) - \gamma_B|$ (see Fig. 3). We will assume then that such surface tension differences can be used to describe the relative intensity of the flow around the front.

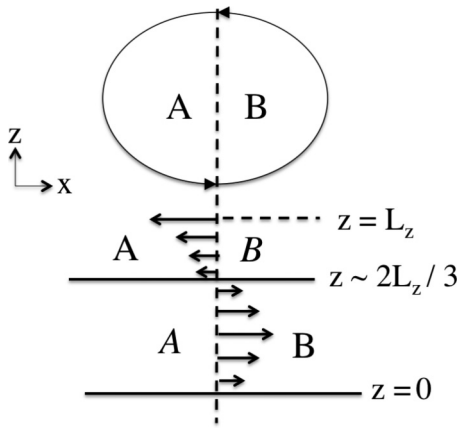

FIG. 9. Schematic structure in depth of the convective roll supposing a parallel fluid flow. The flow initiated at the surface is oriented towards the largest surface tension, i.e., to the left in the present case. A return flow is observed arising from the incompressibility condition. The horizontal component of the flow changes sign around $2L_z/3$. A molecules are pushed to the right due to the action of the return flow in the lower part ($0 < z < 2L_z/3$) while B molecules are driven to the left by the flow near the surface ($2L_z/3 < z < L_z$).

We now define the surface tension differences in the presence of one counterclockwise convective roll by $\Delta\gamma_A = \gamma_A - \gamma(X_f,t)$ and $\Delta\gamma_B = \gamma(X_f,t) - \gamma_B$. If $\Delta\gamma_A > \Delta\gamma_B$, the fluid flow is expected to be more intense on the left-hand side than on the right-hand side and vice-versa. From Eq. (21), we obtain the following equations of evolution:

$$-\partial_t\Delta\gamma_B = \partial_t\Delta\gamma_A = \left(M_a - \frac{M_c}{2}\right)\partial_t a(X_f,L_z,t) + \left(M_b - \frac{M_c}{2}\right)\partial_t b(X_f,L_z,t). \quad (24)$$

As in the RD theory,[1,9] for equal initial concentrations and diffusion coefficients of reactants, we have numerically checked that the reaction front X_f corresponds to the equivalent point where $b(X_f,z,t) \approx a(X_f,z,t)\forall(z,t)$. Eq. (24) becomes then

$$-\partial_t\Delta\gamma_B = \partial_t\Delta\gamma_A = (M_a + M_b - M_c)\,\partial_t a(X_f,L_z,t). \quad (25)$$

While the front always moves initially to the right as explained above, Eq. (25) then predicts three different scenarios for the evolution of the relative intensity of the flow around the front in time and therefore for its subsequent direction of motion. Since $\partial_t a(X_f,L_z,t) \le 0$, (i) if $M_c < M_a + M_b$, the intensity of the flow grows on the right side pushing the front in the opposite direction (front reversal). (ii) If $M_c > M_a + M_b$, the intensity of the flow grows on the left side pushing then the front to the right (no front reversal) and (iii) if $M_c = M_a + M_b$, the relative intensity does not evolve in time (no front reversal). Finally, Eq. (25) shows that as M_c increases to $M_a + M_b$, changes in time of $\Delta\gamma_A$ and $\Delta\gamma_B$ are slower and so the front will take more time to reverse its direction explaining the time delay at which the front reversal occurs in Fig. 8(a). In the limit where M_c tends to $M_a + M_b$ ($M_c \approx M_a + M_b$), the intensity of the flow is not sufficiently stronger on the right side compared to the left side to overcome the initial direction of the front and no reversal occurs. This is the reason why we numerically observe that $M_a = 20, M_b = 40$ and $57 \lesssim M_c < 60$ do not lead to a front reversal either. We note that the reversal of the front direction that we observe is from convective origin and is unrelated to the reversal observed in the case of RD fronts with different initial concentrations of reactants and different diffusion coefficients.[8,9]

C. Summary of the front dynamics in the (M_b, M_c) plane at fixed M_a

From Fig. 2, we can draw the general picture of the front dynamics based on the results obtained in Subsections III A and III B (see Fig. 10). The initial direction of the front propagation is represented by dark filled arrows. The broken line $M_a + M_b \approx M_c$ in the shaded regions separates the subregion where a front reversal (FR) can be observed

Reuse of AIP Publishing content is subject to the terms: https://publishing.aip.org/authors/rights-and-permissions. Downloaded to IP: 164.15.136.4 On: Fri, 07 Oct 2016 12:23:06

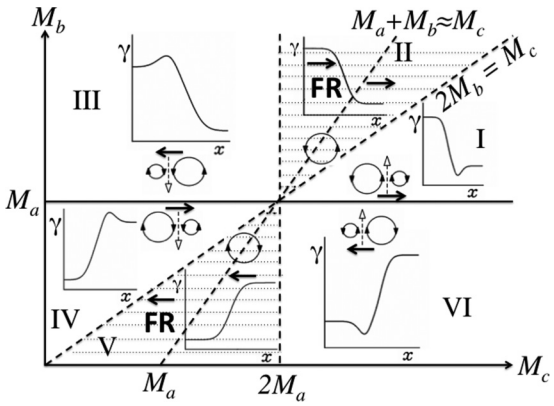

FIG. 10. Classification of the different expected dynamics in the (M_b, M_c) parameter plane at fixed M_a. The dark filled arrow indicates the initial direction of propagation of the front. A front reversal (FR) can only be observed for $M_c < M_a + M_b$ in the presence of one convective roll (shaded regions) (see description of Fig. 2 for additional information about the different regions).

($M_c < M_a + M_b$) from the subregion where no reversal occurs ($M_c > M_a + M_b$). The lower regions (regions IV, V, VI) are obtained straightforwardly from the upper regions (regions III, II, I). By comparing the present classification for the front dynamics with the one obtained in the case of buoyancy-driven convection,[33] we note that the shaded parts of the lower and upper regions are not symmetrically opposed anymore. The Marangoni-driven convection has indeed broken the symmetry associated to the transformation $M_a \leftrightarrow M_b$ in the shaded parts corresponding to one convective roll. Furthermore, the asymmetric surface tension profiles for all the Marangoni numbers in the shaded regions lead to the front propagation as explained above. This is in strong contrast with the buoyancy-driven case where the front is stationary for $R_a + R_b = R_c$ since the density profiles are antisymmetric, with $R_{a,b,c}$ defined as the Rayleigh numbers of each species. Those two main differences arise from the vertical structure of the flow as explained above.

Finally, it is interesting to note that other relevant quantities in this reaction-diffusion-convection system with initially separated reactants, such as the reaction front width or the production rate, do not exhibit such a rich spatiotemporal behavior. That statement has already been pointed out by Koza *et al.* for the pure reaction-diffusion case with different initial concentrations and diffusion coefficients.[8] However, for instance, the reaction front width may behave nonmonotically since the front spreads out more rapidly in the presence of convective motions. It therefore scales in time as $t^{\alpha>1/6}$ in the short-time limit, which is different from the $t^{1/6}$ scaling predicted and observed in the long-time diffusive limit.[1,4]

IV. CONCLUSIONS

The nonlinear dynamics of A + B → C chemical fronts in horizontal solution layers can be influenced by Marangoni-driven convection provided that A, B, and C influence differently the surface tension of the aqueous solution. We have studied the dynamics of such fronts both theoretically and numerically by integrating the 2D incompressible Navier-Stokes equations coupled to reaction-diffusion-convection equations for the concentrations of the three chemical species and for equal initial concentrations and diffusion coefficients. We show that the presence of convection can lead to rich behaviors for the reaction front propagation while the reaction-diffusion models predict a stationary front. The motion of the reaction front in the presence of convection depends on the symmetry properties of the surface tension profiles. Since the surface tension profiles are asymmetric for all the Marangoni numbers (except for $M_a = M_b$, $\forall M_c$), the front moves and its direction of propagation is expected to be oriented towards the smallest surface tension gradient, i.e., the weakest flow. Such an evolution criterion has proven useful to efficiently solve a maze, i.e., find the shortest path between two points in a maze.[37–39] Here, we have shown that such a criterion can be used to predict the position of the front traveling with two convective rolls. However, this criterion cannot explain the front reversal that occurs in the presence of one convective roll for some sets of Marangoni numbers since it does not take into account the large amount of one of the reactants displaced compared to the other one. We have explained the mechanism leading to the front reversal and predicted for which Marangoni numbers it can be observed from analytical arguments. Moreover, we have shown that the layer thickness only affects quantitatively but not qualitatively the front dynamics independently of the number of convective rolls and the sets of Marangoni numbers considered. Based on all those findings, we have proposed a new classification of the front dynamics as a function of the Marangoni numbers (see Fig. 10).

By comparing our results with those obtained for buoyancy-driven convection induced around A + B → C reaction fronts,[33] we conclude that Marangoni-driven convection leads to more complex and exotic dynamics of the front. The main reason for this observation is due to the change of boundary conditions for the fluid velocity field that affects deeply the structure of the fluid flow. Indeed the identical no-slip boundary conditions at the surface and the bottom of a closed system with buoyancy-driven flows allow the system to possess a symmetry around the horizontal axis $z = L_z/2$. The dynamics of the front can then be reduced to a one-dimensional problem depending only on the relative flow intensity around the front. On the other hand, in the presence of an open surface and Marangoni flows, such a symmetry is lost and it follows immediately that one of the reactants is displaced on a larger thickness compared to the other one, making the study of the front dynamics more complex. Those findings emphasize therefore the important role played by flow symmetry properties on convective front dynamics.

Several extensions of this work could be envisioned. First, we could analyze the influence of the reaction exothermicity on the dynamics of the system in both cases of cooperative and competitive solutal and thermal effects which has been shown to lead to oscillatory flow.[40] Moreover, different initial concentrations of reactants and diffusive coefficients will be considered starting from the particular case $a_0\sqrt{D_a} = b_0\sqrt{D_b}$ where the RD front is stationary. Finally, we have assumed sufficiently dilute solutions and written a linear dependence of the surface tension on the concentrations. To extend

Reuse of AIP Publishing content is subject to the terms: https://publishing.aip.org/authors/rights-and-permissions. Downloaded to IP: 164.15.136.4 On: Fri, 07 Oct 2016 12:23:06

the application scope of our model to the realm of high concentrations, it would be natural to consider next nonideal models and more complex dependences of the solution properties on the concentrations.

ACKNOWLEDGMENTS

The authors thank the "Actions de Recherches Concertées" program and the F.R.S.-FNRS for their financial support. We thank A. De Wit and V. Voorsluijs for their useful comments about this work.

[1]L. Gálfi and Z. Rácz, Phys. Rev. A **38**, 3151 (1988).
[2]Z. Jiang and C. Ebner, Phys. Rev. A **42**, 7483 (1990).
[3]S. Cornell, Z. Koza, and M. Droz, Phys. Rev. E **52**, 3500 (1995).
[4]Z. Koza, J. Stat. Phys. **85**, 179 (1996).
[5]K. H. Stern, Chem. Rev. **54**, 79 (1954).
[6]P. V. Danckwerts, Trans. Faraday Soc. **46**, 701 (1950).
[7]P. M. J. Trevelyan, D. E. Strier, and A. De Wit, Phys. Rev. E **78**, 026122 (2008).
[8]Z. Koza and H. Taitelbaum, Phys. Rev. E **54**, R1040 (1996).
[9]H. Taitelbaum, Y.-E. L. Koo, S. Havlin, R. Kopelman, and G. H. Weiss, Phys. Rev. A **46**, 2151 (1992).
[10]Y.-E. L. Koo, L. Li, and R. Kopelman, Mol. Cryst. Liq. Cryst. **183**, 187 (1990).
[11]Y.-E. L. Koo and R. Kopelman, J. Stat. Phys. **65**, 893 (1991).
[12]A. Yen, Y.-E. L. Koo, and R. Kopelman, Phys. Rev. E **54**, 2447 (1996).
[13]T. A. Gribschaw, K. Showalter, D. L. Banville, and I. R. Epstein, J. Phys. Chem. **85**, 2152 (1981).
[14]G. Bazsa and I. R. Epstein, J. Phys. Chem. **89**, 3050 (1985).
[15]I. Nagypál, G. Bazsa, and I. R. Epstein, J. Am. Chem. Soc. **108**, 3635 (1986).
[16]H. Miike, S. C. Müller, and B. Hess, Phys. Rev. Lett. **61**, 2109 (1988).
[17]J. A. Pojman and I. R. Epstein, J. Phys. Chem. **94**, 4966 (1990).
[18]H. Miike and S. C. Müller, Chaos **3**, 21 (1993).
[19]M. J. B. Hauser and R. H. Simoyi, Phys. Lett. A **191**, 31 (1994).
[20]S. H. Park, S. Parus, R. Kopelman, and H. Taitelbaum, Phys. Rev. E **64**, 055102(R) (2001).
[21]B. S. Martincigh and R. H. Simoyi, J. Phys. Chem. A **106**, 482 (2002).
[22]Y. Shi and K. Eckert, Chem. Eng. Sci. **61**, 5523 (2006).
[23]A. Pereira, P. M. J. Trevelyan, U. Thiele, and S. Kalliadasis, J. Eng. Math. **59**, 207 (2007).
[24]A. Pereira, P. M. J. Trevelyan, U. Thiele, and S. Kalliadasis, Phys. Fluids **19**, 112102 (2007).
[25]C. Almarcha, P. M. J. Trevelyan, P. Grosfils, and A. De Wit, Phys. Rev. Lett. **104**, 044501 (2010).
[26]L. A. Riolfo, J. Carballido-Landeira, C. O. Bounds, J. A. Pojman, S. Kalliadasis, and A. De Wit, Chem. Phys. Lett. **534**, 13 (2012).
[27]K. Eckert, L. Rongy, and A. De Wit, Phys. Chem. Chem. Phys. **14**, 7337 (2012).
[28]A. De Wit, K. Eckert, and S. Kalliadasis, Chaos **22**, 037112 (2012).
[29]L. Šebestíková and M. J. B. Hauser, Phys. Rev. E **85**, 036303 (2012).
[30]E. Pópity-Tóth, V. Pimienta, D. Horváth, and A. Tóth, J. Chem. Phys. **139**, 164707 (2013).
[31]J. A. Pojman, I. R. Epstein, T. J. McManus, and K. Showalter, J. Phys. Chem. **95**, 1299 (1991).
[32]D. Horváth, M. A. Budroni, P. Bába, L. Rongy, A. De Wit, K. Eckert, M. J. B. Hauser, and A. Tóth, Phys. Chem. Chem. Phys. **16**, 26279 (2014).
[33]L. Rongy, P. M. J. Trevelyan, and A. De Wit, Phys. Rev. Lett. **101**, 084503 (2008).
[34]L. Rongy, P. M. J. Trevelyan, and A. De Wit, Chem. Eng. Sci. **65**, 2382 (2010).
[35]A. A. Nepomnyashchy, M. G. Velarde, and P. Colinet, *Interfacial Phenomena and Convection* (Chapman and Hall/CRC, Boca Raton, 2002).
[36]L. Rongy and A. De Wit, J. Chem. Phys. **124**, 164705 (2006).
[37]I. Lagzi, S. Soh, P. J. Wesson, K. P. Browne, and B. A. Grzybowski, J. Am. Chem. Soc. **132**(4), 1198 (2010).
[38]K. Suzuno, D. Ueyama, M. Branicki, R. Tóth, A. Braun, and I. Lagzi, Langmuir **30**(31), 9251 (2014).
[39]P. Lovass, M. Branicki, R. Tóth, A. Braun, K. Suzuno, D. Ueyama, and I. Lagzi, RSC Adv. **5**, 48563 (2015).
[40]L. Rongy, P. Assemat, and A. De Wit, Chaos **22**, 037106 (2012).

Reuse of AIP Publishing content is subject to the terms: https://publishing.aip.org/authors/rights-and-permissions. Downloaded to IP: 164.15.136.4 On: Fri, 07 Oct 2016 12:23:06